Stiffness-Mediated Adhesion of Cervical Cancer Cells to Soft Hydrogel Films

*James P. Best, Sameen Javed, Joseph J. Richardson, Kwun Lun Cho, Marloes M. J. Kamphuis and Frank Caruso**

Department of Chemical and Biomolecular Engineering, The University of Melbourne, Parkville, Victoria 3010, Australia. Fax: +61 3 8344 4153; Tel: +61 3 8344 3461; E-mail: fcaruso@unimelb.edu.au

Supplementary Information

Materials and Methods

The pH of all solutions was measured with a Mettler-Toledo MP220 pH meter. High purity (Milli-Q) water with a resistivity of > 18 MΩ·cm^{-1} was obtained from an inline Millipore RiOs/Origin water purification system. Dialysis tubing (68035-35FT) with a MWCO of 3500 Da was obtained from Thermo Scientific. Poly(methacrylic acid, sodium salt), (PMA-Na, M_W = 15 000 g mol^{-1}) was purchased from Polysciences, and PVPON (M_W = 10 000 g mol^{-1}), 1-Ethyl-3-(3-dimethylaminopropyl)carbodiimide (EDC), dithiothreitol (DTT), polyethyleneimine (PEI, 25 000 g mol^{-1}), phosphate buffered saline (PBS), 3-(*N*-morpholino)propanesulfonic acid (MOPS), 2-(*N*-morpholino)ethanesulfonic acid (MES), sodium acetate (NaOAc), *N*-chloro-*p*-toluenesulfonamide sodium salt (CaT) and pyridine dithioethylamine hydrochloride (PDA) were obtained from Sigma-Aldrich. All chemicals were used as received. Mica (grade V-4) and Thermanox planar substrates of 22 mm diameter were sourced from SPI Chem (USA), and ProSciTech (Australia), respectively. Nuclear magnetic resonance (NMR) spectra were recorded using a 500 MHz Varian INOVA system at 25 °C. Spectra were referenced to residual proton

resonances of the deuterated solvent. Chemical shifts are reported as parts per million (ppm) downfield from the signal origination of TMS.

PMA_{SH} Synthesis

PMA-Na (100 mg) was dissolved in a filtered (0.2 µm) and deoxygenated (N_2 (g) stream, 15 min) PBS solution (25 mL, 100 mM, pH 7.4). PDA was added in a stoichiometric excess of 1.75 equivalents of the target PDA percentage and EDC in a stoichiometric excess of 2.90 equivalents under stirring at 24 °C, to obtain 5, 10, 15, and 20 mol % target modifications. The resulting solution was stirred at 24 °C for 18 h under a N_2 (g) atmosphere, after which the solution was dialysed (MWCO 3500 Da) against Milli-Q water over a period of 5 days, with frequent exchange of the dialysis solution. The resulting purified solution was freeze-dried to give PMA-PDA as a white solid. ^{1}H NMR (500 MHz, D_2O): δ 8.42 (s, broad, 1H, Ph), 7.81 (s, broad 1H, Ph), 7.68 (s, broad, 1H, Ph), 7.32 (s, broad 1H, Ph), 3.59-3.31 (multiplet, broad, 2H, NCH_2) 3.21-3.03 (multiplet, broad, 2H, CH_2S) and 2.93 (s, broad 2H, CH_2S), (d, J = 5.8 Hz, 2H, CH_2), 1.91-1.72 (multiplet, 4H, CH_2), 1.27-0.73 (multiplet, 6H, CH_3). ^{13}C NMR (125 MHz, D_2O/d_6-DMSO 6:1): δ 187.9 (CO), δ 182.2 (CO, substituted), 161.8 (Pyr), 150.8 (Pyr), 140.2 (Pyr), 123.5 (Pyr), 106.4 (Pyr), 56.6 (CH_2), 47.2 (C), 38.0 (CH_2, PDA), 36.3 (CH_2, PDA), 26.4 (C, substituted), 18.7 (CH_3), 16.2 (CH_3, substituted). Through integration of the peaks at 1.91-1.72, and 1.27-0.73 ppm and the aromatic signals at 8.42, 7.81, 7.68, and 7.32 ppm the extent of PDA modification in the PMA-PDA samples that are the precursors for the $PMA_{SH(\mathbf{5})}$, $PMA_{SH(\mathbf{10})}$, and $PMA_{SH(\mathbf{15})}$ polymers could be determined. The solubility of the PMA-PDA precursor for $PMA_{SH(\mathbf{20})}$ is insufficient in D_2O, hence the ^{1}H-NMR spectrum was recorded in d_6-DMSO. δ 8.47 (s, broad 1H, Ph), 7.83 (s, broad 1H, Ph), 7.77 (s, broad, 1H, Ph), 7.24

(s, broad 1H, Ph), 3.31 (s, broad, 2H, NCH_2 plus HDO peak), 2.86 (s, broad, 2H, CH_2S), 2.08 (s, broad) and 1.32-0.63 (multiplet, broad, 26H, CH_2 and CH_3)**.**

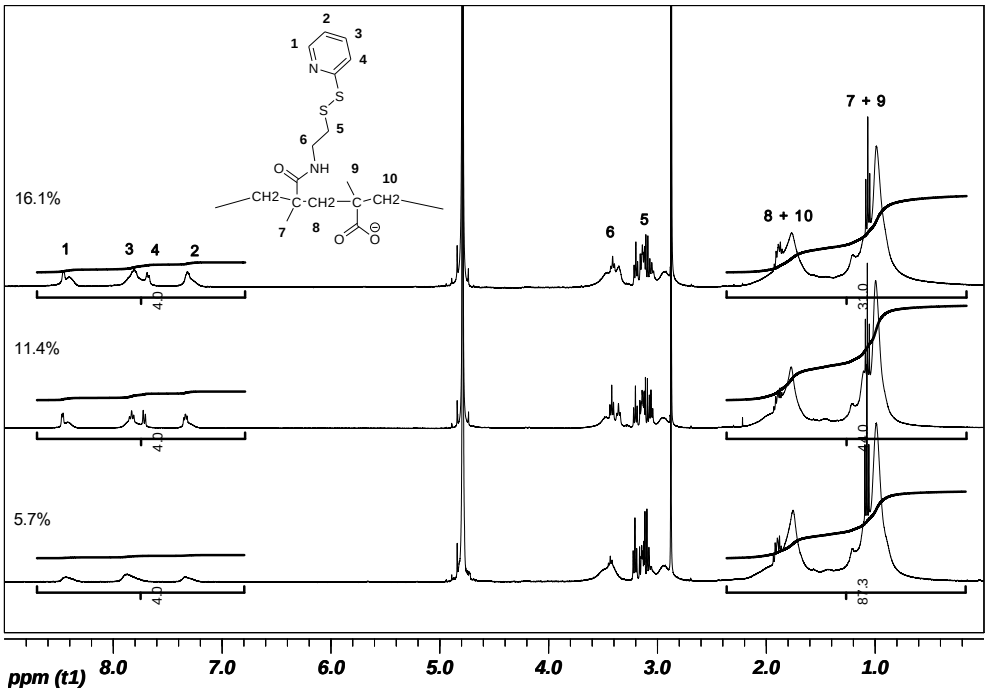

Figure S1. ^{1}H-NMR spectra of PMA-PDA in D_2O.

Next, the PMA-PDA precursor was reduced to PMA_{SH} through cleavage of the PDA group. The reduction required a 0.5 M DTT solution in 50 mM MOPS buffer (pH 8) at 37 °C for 30 min with constant agitation. The resultant PMA_{SH} solution was then diluted with 100 mM NaOAc buffer (pH 4) to 0.5 mg mL^{-1}.

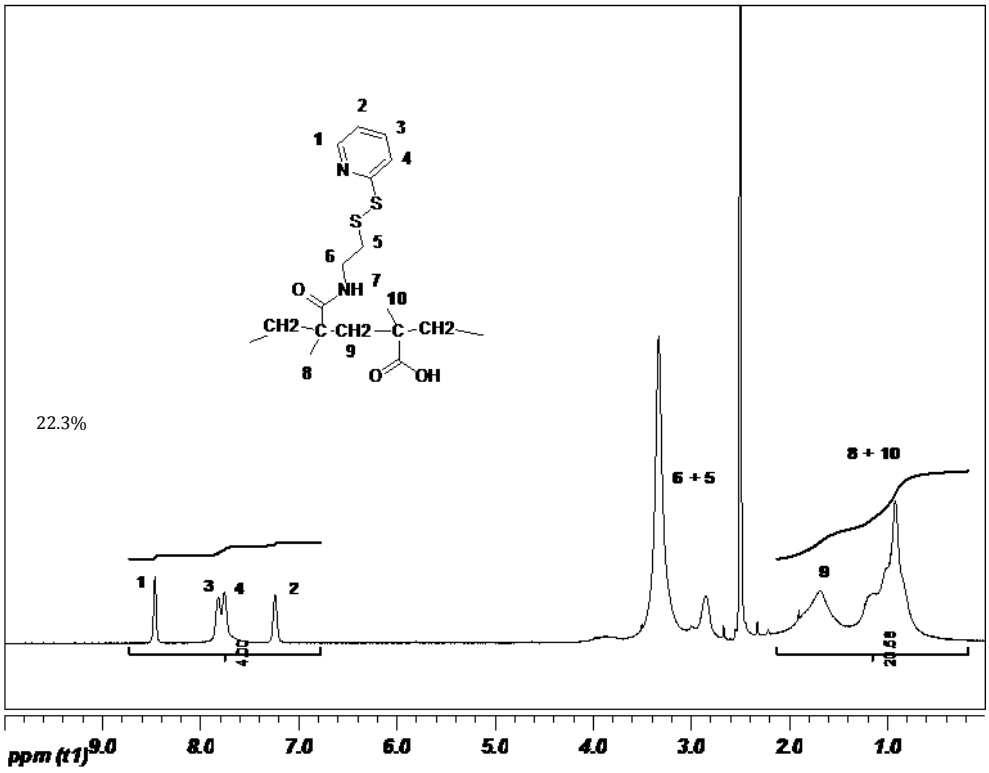

Figure S2. ^{1}H-NMR spectra of PMA-PDA in d_6-DMSO.

PMA_{SH} Film Fabrication

For layering onto mica and Thermanox substrates, an initial monolayer of PEI (1 wt. %) was adsorbed to promote PMA_{SH} adhesion. Alternating layers of PMA_{SH-x} and PVPON (300 µL, 0.5 mg mL^{-1} in 100 mM NaOAc buffer) were then adsorbed until five layers of PMA_{SH-x} were deposited. Between each polymer deposition step, the substrate wells were washed by mild agitation with NaOAc buffer (3 x 300 µL). The films were then oxidised using CaT (5 mM) in MES buffer (10 mM, pH 6) for 10 min. The PVPON was kept within the assembly until use, where it was removed by washing with PBS (12.2 mM, pH 7.4, 140 mM NaCl) (3 x 300 µL).

AFM Characterisation

Both intermittent contact (IC) mode and CP cantilevers were cleaned to remove salt deposition and organic material prior to use. The cantilevers were immersed in a 30 vol. % isopropanol solution, followed by Milli-Q water, and then further cleaned using oxygen plasma for 180 s (Harrick Plasma, 0.1 L min^{-1} O_2 flow rate, 29.6 W, 300 mTorr). Glass substrates for cantilever spring constant calibration were cleaned using the same method.

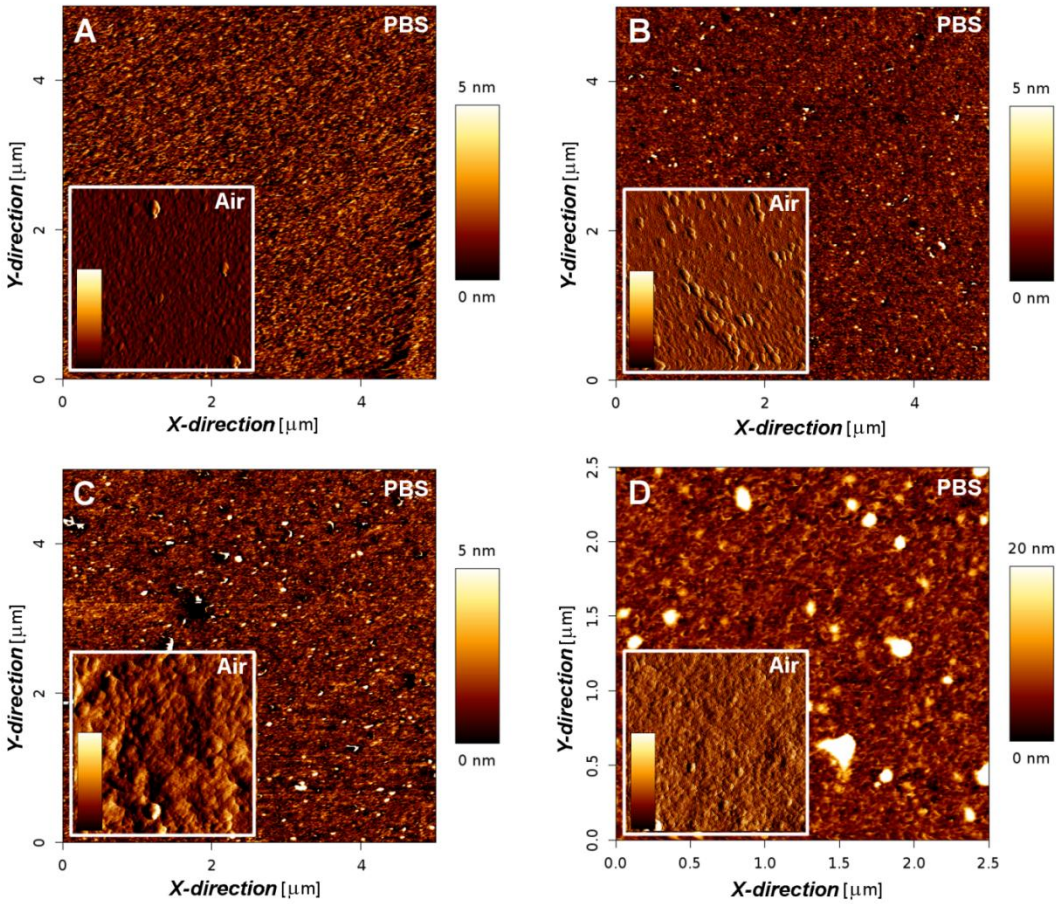

Figure S3. Tapping mode images of PMA_{SH} films in both PBS buffer and air (insets). Images **A**, **B**, **C** and **D** represent 5, 10, 15 and 20 mol % $PMA_{SH(x)}$ films, respectively.

For IC mode imaging of film structures in air, standard tapping mode cantilevers with a spring constant of 40 N m^{-1} (Tap300-G, Budget Sensors, Bulgaria) were used. For IC mode imaging of PMA_{SH} films in PBS buffer, softer cantilevers with a nominal spring constant of 0.3 N m^{-1} (CSC37, MikroMasch, Estonia) were employed while oscillating the cantilevers at *ca*. 10 kHz. Images were recorded using a JPK Nanowizard II (JPK Instruments AG, Berlin, Germany) and shown in Figure S3. Images were post-treated using accompanying JPK image processing software and in-built algorithms. A three-point 1st degree polynomial fit was first subtracted, and then a polynomial fit subtracted from each scan line independently. It was found that due to film contraction upon drying PMA_{SH} films were not stable in air, with the exception of $PMA_{SH(20)}$, as shown in Figure S3. This was attributed to the increased number of stabilising crosslinks in the 20 mol % modified film. For determination of the roughness ratio (*r*), IC height images for the surfaces in buffer were analysed using SPIP software (Image Metrology A/S, Denmark). Results are shown below in Table S1. A general increase in *r* is seen as polymer modification increases, possibly due to the increasingly hydrophobic nature of the polymer chain and film (evidenced in Figure 2, main text). This may lead to the hydrophobic polymer 'clustering' on the surface seen in Figure S3.

Table S1. Roughness ratio values for $PMA_{SH(x)}$ films and substrates in PBS buffer.

	Mica	PEI-mica	$PMA_{SH(5)}$	$PMA_{SH(10)}$	$PMA_{SH(15)}$	$PMA_{SH(20)}$
r	1.0005	1.0002	1.0048	1.0037	1.0086	1.0425

Force spectroscopy measurements were carried out in PBS (140 mM NaCl, pH 7.4) buffer using a JPK Nanowizard II AFM. For fabrication of the colloidal probe modified cantilevers, tipless cantilevers (CSC12 (tipless/no Al), MikroMasch, Estonia) were first

calibrated on a cleaned glass substrate to calculate the Inverse Optical Lever Sensitivity (InvOLS) as described in literature [1]. A spherical glass bead (30 to 50 µm diameter, Polysciences Inc., USA) was attached to the calibrated cantilever using an epoxy resin (UHU Plus endfest 300, UHU & Co. KG, Germany) via careful manual manipulation using the AFM and associated optics. After overnight drying of the resin, cantilevers with spring constants of 7.3 ($PMA_{SH(\mathbf{5})}$), 14.1 ($PMA_{SH(\mathbf{10})}$ and $PMA_{SH(\mathbf{15})}$) and 36.4 mN m^{-1} ($PMA_{SH(\mathbf{20})}$) were employed. For force measurements on hydrogel films, the InvOLS for each cantilever was first calibrated on PEI-coated mica in PBS buffer. The force measurements on the films were then undertaken over a 50 x 50 μm^2 area, with 25 data points collected, to give an indication of film homogeneity. The approach speed was kept constant, at 300 nm s^{-1} for all measurements.

Film Characterisation

ζ-potential measurements were carried out in Milli-Q water adjusted to pH 7.4 using a Zetasizer Nano ZS (Malvern) on 5 µm-diameter colloidal silica particles, with the films prepared using the same conditions as those used to prepare the films on planar surfaces. Inverse captive bubble measurements were performed using a Model 200 Standard Goniometer (Ramé-Hart, USA) with a microsyringe attachment at an ambient temperature (25 °C). A small air bubble (~20 µL) was introduced via a microsyringe and brought into contact from below, with a coated mica sample submerged in Milli-Q water with the coated side facing down. The digitised image of the bubble-surface contact point, captured via CCD camera (as shown in Figure S4), was analysed using DROPimage series software (Ramé-Hart, USA) to determine the tangential apparent contact angle (θ^*). Each recorded measurement was an average of 5 images taken at 0.2 s intervals.

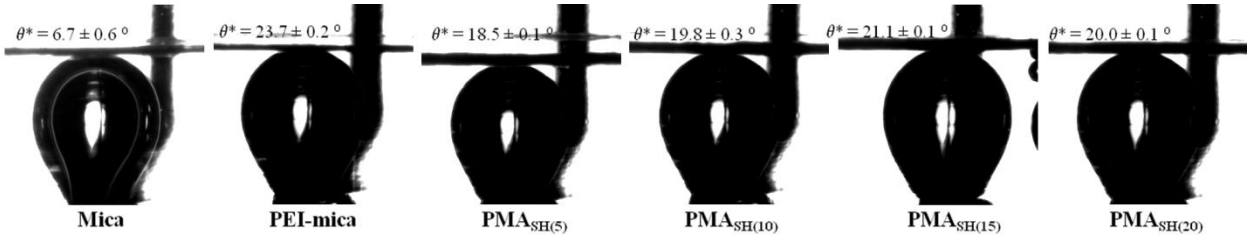

Figure S4. CCD images of inverse captive air bubbles on mica and PMA$_{SH(x)}$ polymer films.

Combining the apparent contact angle (θ*), with the roughness factor (r) determined from AFM image analysis, according to the Wenzel equation, the Young's contact angle (θ_{Young}) describing an idealised smooth surface of homogeneous chemistry was calculated according to:

$$\cos\theta^* = r\cos\theta_{Young} \quad (1)$$

HeLa Cell Adhesion Measurements

HeLa cells were trypsinised and 5 x 10^6 cells were resuspended in 5 mL of PBS buffer at 37 °C. HeLa cells were then labelled with 15 µM Vybrant CFDA SE (Invitrogen) and incubated for 15 min at 37 °C in a 5% CO_2 humidified atmosphere. Cells were centrifuged (5 min, 400 *g*) and resuspended in DMEM media (Gibco) containing 10% FBS and 1% Glutamax. Cells were plated in 12 well plates at a concentration of 0.6 x 10^6 cells per well (2 mL per well). After 6 h incubation at 37 °C in a 5% CO_2 humidified atmosphere, cells were washed 3 times with PBS (pre-heated to 37 °C) with moderate agitation. To count adherent HeLa cells, washed films were observed under an Olympus IX71 microscope at 10 times magnification, with fluorescent light at 488 nm. Cells were easily visible due to the Vybrant labelling, and counted manually using ImageJ software. At least five representative images were taken for each sample, and used for

data analysis. Control experiments were performed for each of the four hydrogel films fabricated on both mica and Thermanox substrates. As seen in Figure S5 (left), there was negligible difference between using the two substrates. Thermanox showed slightly lower adhesion properties for all films, but these small differences may be attributed to experimental deviations in seeding out 0.6 x 10^6 cells to each well, as all results are within error. The difference between commercial cell growth substrates and PMA_{SH} films was also studied. Bare mica, cell culture wells (CCW) and Thermanox (Th-nx) substrates, and $PMA_{SH(\mathbf{20})}$ films on the aforementioned substrates were tested for HeLa cell adhesion properties. As can be seen in Figure S5 (right), adhesive properties were within error between bare cell-culture substrates and 20 mol % modified PMA_{SH} films over a 6 h incubation period.

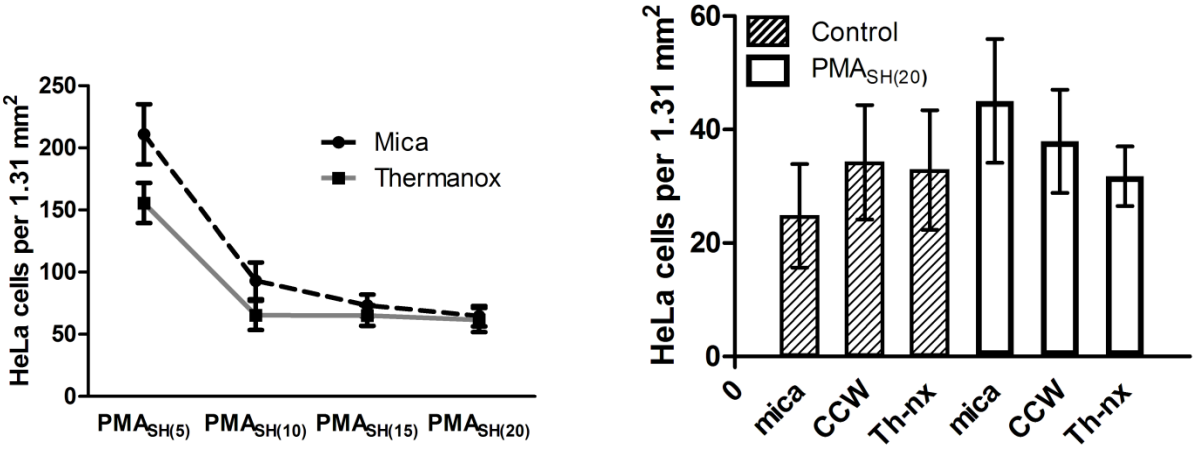

Figure S5. Adhesion comparison between hydrogel films fabricated on both mica and Thermanox substrates (left), and control experiment showing HeLa adhesion to bare growth substrates and $PMA_{SH(\mathbf{20})}$ films (right). Error bars represent one standard deviation.

Mathematical Modelling

Force Curve Treatment

Raw AFM data was processed using JPK data processing software to subtract the zero-force baseline, shift the data along the deformation axis to zero the initial contact point, and to export force data. The effect of cantilever bending during sample compression was removed to give true sample deformation data, as outlined in equation 2,

$$\delta = \text{Displacement} - {}^{F}/_{k_c} \qquad (\mathbf{2})$$

where k_c is the spring constant of the cantilever. For an incompressible material, the force increases with no observable change in deformation, while for softer samples the gradient reduces due to the compliance of the material. Due to possible viscoelastic effects and associated hysteresis, only the approach force curve was analysed. Example approach and retract curves for the four planar hydrogel films studied are shown in Figure S6. The stiffness was evaluated to be the slope of the force/deformation curve in the small-deformation regime (approximately 40 nm) as can be seen in Figure 3. Reported stiffness values are an average of at least 20 separate measurements, with the error equating to one standard deviation of the data set. For the colloidal probe cantilevers used, there was only a small variation in probe radius (16.5 ± 2.0 μm) and the effect of differences in contact area between samples was discounted. Figure S6 (left) shows full-range F-δ curves where both the contact point and point of substrate incompressibility can be seen, allowing for an estimation of hydrogel film thicknesses. As can be seen from the figure, no trends were observed for hydrogel films with increasing crosslinking. Analysis of the F-δ data gives a general film thickness of 130 ± 50 nm for all PMA modifications. It is possible that more

highly crosslinked films are more stable and retain more polymer material while resisting expansion at pH 7.4, leading to a complex relationship between crosslinking and film thickness. In addition, from Figure S6 (right) it was observed that the maximum pull-off force (F_{PO}) increased with decreasing crosslinker, which could also be reasoned with the decreasing stability and network density of the hydrogel films.

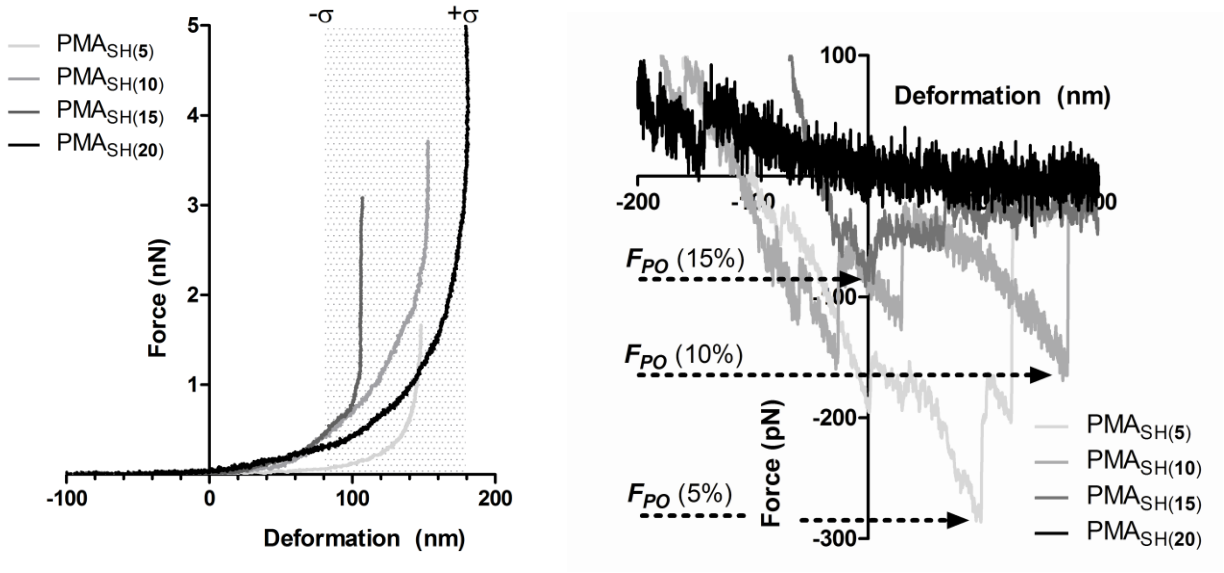

Figure S6. Full-range force-indentation curves for planar hydrogel films on mica (left), and force-retract curves (right) showing the adhesive properties of the PMA_{SH} films. The gray area depicts standard deviation (± σ) limits for hydrogel film thicknesses for all PMA modifications.

Hertz and JKR E_Y Modelling

The Young's modulus (E_Y) of the PMA_{SH} films was calculated using both Hertz and JKR modelling approaches. Hertzian fits to the experimental data was performed using JPK data processing software and in-built algorithms, using Equation 3 for an incompressible spherical

indenter. A Poisson ratio (ν) of 0.5 was assumed for all calculations, a common literature assumption for incompressible isotropic elastic materials [2], according to:

$$E_Y = \frac{3F\left(1-\nu^2\right)}{4R^{0.5}\delta^{1.5}} \quad \textbf{(3)}$$

As evidenced in Figure S7, PMA_{SH} films demonstrated relative mechanical homogeneity over a large surface area, with little deviation seen for films fabricated onto mica or Thermanox substrates. This also demonstrated that the substrate had negligible effect on the film mechanical properties, and correlates well with HeLa adhesion results presented in Figure S5. E_Y values evaluated using Hertzian theory increased from 0.34 to 2.13 kPa as thiol modification increased for the four hydrogel films. However, it was judged that pure Hertzian theory was not appropriate in this case, due to moderate non-zero adhesive interactions occurring between the probe and sample. This adhesive interaction is shown in Figure S6 (right), and it should be noted that the magnitude of the interaction increased significantly as the crosslinking extent, and film stiffness, decreased.

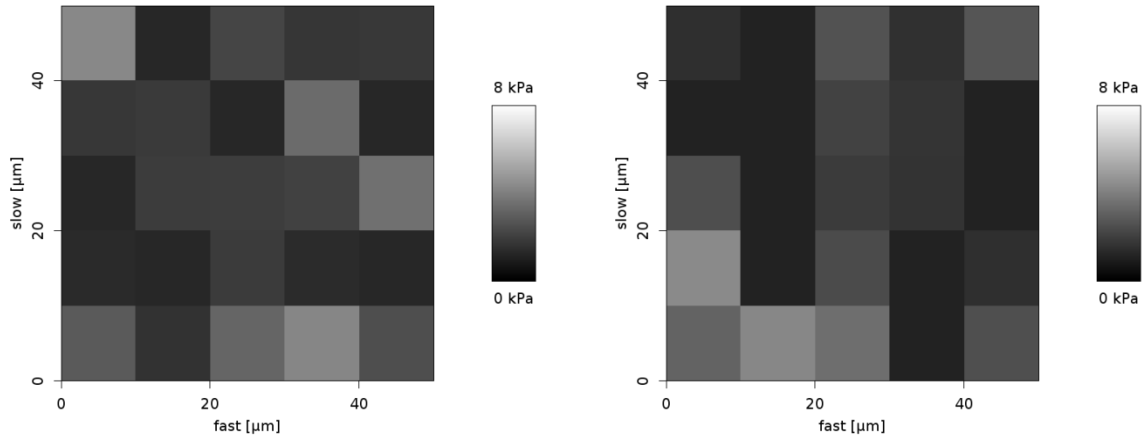

Figure S7. 50 x 50 µm^2 E_Y maps for $PMA_{SH(\mathbf{20})}$ films on mica (left) and Thermanox (right).

In addressing this, a JKR model was employed (equations 4 and 5), taking into account adhesive interactions between probe and sample. The work of adhesion ($W_{adh.}$) is defined as the area under the retract-curve in the attractive force regime, and was quantified for all samples using equation 6, where F_{PO} is the maximum pull-off force.

$$a^3 = \frac{3R(1-\nu^2)}{4E_Y}\left(F + 3W_{adh.}\pi R + \sqrt{6W_{adh.}\pi RF + (3W_{adh.}\pi R)^2}\right) \quad (4)$$

$$\lambda = F + 3W_{adh.}\pi R + \sqrt{6W_{adh.}\pi RF + (3W_{adh.}\pi R)^2} \quad (5)$$

$$W_{adh.} = \frac{2F_{PO}}{3\pi R} \quad (6)$$

$$\delta = \frac{a^2}{3R} + \frac{F(1-\nu^2)}{2aE_Y} \quad (7)$$

$$a = \left[\frac{3R\lambda\delta}{2F+\lambda}\right]^{0.5} \quad (8)$$

Combining equations 4 and 7 using algebraic techniques, a term for the contact area (a) could be elucidated (equation 8). Using collected force (F) deformation (δ) data for the four films, point-E_Y values were plotted against deformation distance, as shown in Figure S8 below. The data was also plotted over the full extent of film indentation (Figure S8, right) in order to monitor the influence of substrate rigidity on the hydrogel films. Large point-E_Y values at small indentations are a result of uncertainties in contact point determination, combined with energy dissipation upon initial probe/film contact. We would expect substrate effects to play a role from *ca*. 10% of indentation. Observations for the PMA_{SH} hydrogel films suggest, however, that it is generally after indentations of 40 to 50% of film thickness that this is the case.

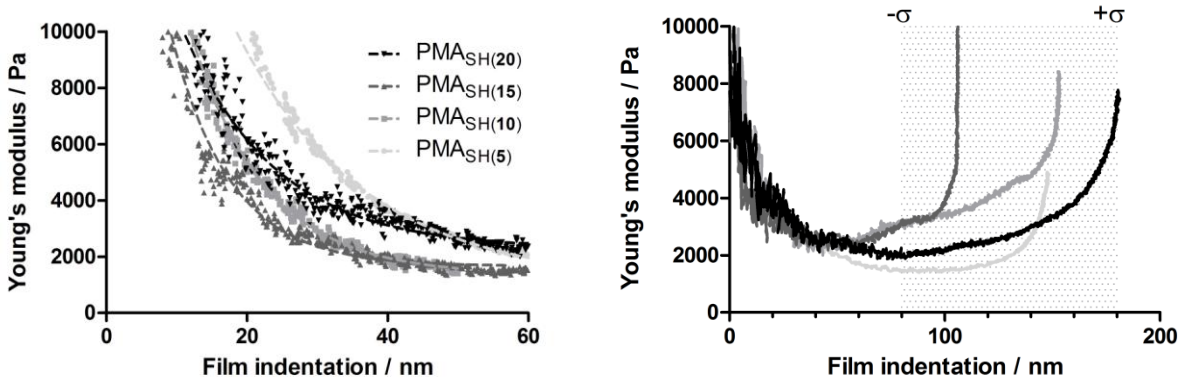

Figure S8. JKR-modelled point-E_Y values for the four hydrogel films on mica, as a function of indentation depth. Small-indentation data (left) with a one phase decay model for EY plateau determination, and full-range data (right) where the gray area depicts standard deviation (± σ) limits for hydrogel film thicknesses.

Using Prism software (GraphPad Software, Inc., USA), point-E_Y data for each series were fit with a one phase decay model, and the E_Y plateau values evaluated, as shown in Table S2. Plateau values signified when the E_Y had reached stability for each force measurement. Low indentation E_Y points are not yet stable due to force-resistance effects caused by initial film contact, such as yield stress and surface energy barriers.

Table S2. Parameters used, and E_Y results, for JKR modelling of hydrogel films. The error in E_Y is represented by one standard deviation.

	$PMA_{SH(5)}$	$PMA_{SH(10)}$	$PMA_{SH(15)}$	$PMA_{SH(20)}$
R (μm)	13.75	18.05	18.05	16.20
F_{PO} (pN)	243.0	124.0	60.8	56.7
E_Y (kPa)	1.05 ± 0.01	1.34 ± 0.05	1.66 ± 0.04	2.27 ± 0.07

Cell/Film Contact Area Modelling

In order to calculate the indentation depth of a non-adhered static HeLa cell on the PMA_{SH} films, a number of assumptions were made: 1) Cells kept a constant spherical morphology. 2) Cell diameter was 13.2 µm (1200 μm^3), with individual cell mass of 1.905 x 10^{-9} g [3]. 3) The hydrogel films act like a spring, with film stiffness equivalent to the spring constant. 4) There are no substrate effects over the deformation range. 5) Cell/film contact height is $\delta + 0.1\delta$ to account for adhesive contact film-lipping effects. 6) Media density is assumed to be 1000 kg m^{-3}.

From these assumptions, both the weight (F_{weight}) and buoyancy ($F_{buoyancy}$) forces could be calculated from equations 9 and 10 below, where V_{cell} is the volume of a single cell, ρ_{media} is the density of media, and g is the gravitational constant.

$$F_{weight} = m_{cell}g \quad \textbf{(9)}$$

$$F_{buoyancy} = V_{cell}\rho_{media}g \quad \textbf{(10)}$$

The total force applied by the cell on the film is the difference between F_{weight} and $F_{buoyancy}$. When combined with the spring constant of the film (k_{film}), the indentation depth (δ) of a static cell can be calculated. It was found that model static HeLa cells 'sink' approximately 10 nm into the hydrogel film. From the indentation depth, the cell/film contact area could be calculated as for a partial sphere (equation 11). It was found that the contact area increased dramatically with decreasing film spring constant. Errors associated with the contact area were due to uncertainties in k_{film}.

$$Contact\ area = 2\pi R_{cell}(\delta + 0.1\delta) \quad (\mathbf{11})$$

References

[1] P. Attard, *J. Physics: Condensed Matter* 2007, **19**, 473201.

[2] C. Quilliet, C. Zoldesi, C. Riera, A. Blaaderen and A. Imhof, *European Phys. J. E* 2008, **27**, 13-20.

[3] R. I. Freshney, *Culture of Animal Cells: A Manual of Basic Technique and Specialized Applications*. Wiley: 2011.